ADVANCED OPTICAL MATERIALS
www.advopticalmat.de

Low-Temperature Synthesis of Silicon Oxynitride-Doped Si for Tunable Bragg Gratings Homogeneously Deposited on Si, SiO_2, and Borosilicate Substrates and the tip of SM and PM Optical Fibers

Ali Karatutlu, Timuçin Emre Tabaru, and Bülend Ortaç*

Optical tunability and repeatability are essential in fabricating optoelectronic devices from waveguides to Bragg gratings (BGs) for high-energy, high-power, mode-locking, and sensing applications. For this purpose, a controlled adjustment in the optical properties, including the refractive index of the deposited nanolayers, becomes critical. This study reveals that silicon oxynitride (SiON) doping into silicon (Si) offers a new way for the preparation of novel Si-based devices with an emphasis on the BGs for filtering a particular portion of an electromagnetic spectrum, including the wavelengths of 800, 976, 1550, and 1840 nm. Control on the incident angle dependence of the BGs is demonstrated at Watt-level for the wavelength of 976 nm. Amorphous SiON-doped Si layers on alternating SiO_2 can be synthesized on bulk substrates and different optical fibers at relatively low temperatures with wide and narrow bandwidths. The high reflectivity of the novel Si-based BGs reveals over −22 dB reflection using typical optical fibers, including standardsingle-mode fibers and high-birefringent polarization-maintaining (PM) fibers. The polarized transmission measurement over the BG on the PMfiber shows the BGs do not deteriorate the PM properties, strongly yielding a beat length of 1.68 mm and birefringence of 9.2×10^{-4} at the telecom C band.

1. Introduction

Earlier works on silicon (Si)[1–6] stimulated the progress in numerous Si-photonics devices, including vertical-cavity surface-emitting lasers (VCSELs),[7] distributed feedback (DFB) lasers[8] and efficient nanophotonic antennas,[9] supercontinuum generation,[10] and optoacoustic detection.[11] Within these photonic devices, Bragg gratings (BGs) are critical and used to improve the efficiency of the devices.

With the insertion of the nitrides within the silicon photonics technology, silicon nitride has become CMOS compatible, and controlled modulation of the light in the visible and NIR windows has been successful.[12,13] Another important area realized by Si photonics is miniaturized spectroscope sensors using Si and Si_3N_4-based on-chip devices.[14] Furthermore, low-temperature deposition of nitrides together with oxides followed the formation of silicon oxynitrides (SiO_xN_y) and for changing the stoichiometry of the compound so that one can control the refractive index of the film.[15] This occurs due to an increase in the hydrogen content in silicon oxynitrides similar to hydrogenated amorphous silicon (a-Si:H) and also leads to a decrease in the optical bandgap.[16]

Due to the small size, lightweight, and strong anti-electromagnetic interference ability of optical fibers, some approaches[17] to transfer the micro- and nano-optical structures to the optical fiber facets were demonstrated and successfully used in spectral sensing.[18] One report studied the direct deposition of BGs on asingle-mode fiber (SMF) using electron beam deposition technique, nevertheless, the study was demonstrated for the single application wavelength with the reflection values of 50–80% (3–7 dB respectively).[19] Despite all the progress in Si photonics, a great challenge remains in the quest to direct transfer the high-reflective BG structure on the tip of a typical SMFthat has a cladding diameter of 125 μm. Furthermore, the BGs on the facet of other types of specialty fibers such as polarization-maintaining (PM) fibers are not investigated on the polarization-maintaining properties such as their birefringence.

A. Karatutlu, T. E. Tabaru, B. Ortaç
Institute of Materials Science Nanotechnology and National Nanotechnology Research Center (UNAM) Bilkent University
Ankara 06800, Turkiye
E-mail: ali@unam.bilkent.edu.tr
T. E. Tabaru
Sivas University of Science and Technology
Mecnun Otyakmaz Street No:1, Sivas 58100, Turkiye
T. E. Tabaru
Erciyes University
Clinical Engineering
Research and Application Center
Kayseri 38019, Turkiye

The ORCID identification number(s) for the author(s) of this article can be found under https://doi.org/10.1002/adom.202300094

DOI: 10.1002/adom.202300094

This study demonstrates for the first time the low-temperature synthesis of silicon oxynitride-doped a-Si by plasma-enhanced chemical vapor deposition technique and control in the refractive index and reflection of a single silicon oxynitride (SiON)-doped a-Si film. Moreover, SiON-doped Si-containing BGs were fabricated on different bulk substrates including Si, SiO_2 glass, and borosilicate glass for a tunable high reflection of the light with a large bandwidth at different central wavelengths from 800 nm to ≈2 μm. On top of the conventional approaches, such as the fabrication of optical structures and their transfer to optical fiber tips, this study shows nano- to micro-scale films can be directly grown on the tip of different optical fibers such as SMFs and PM optical fibers (PMFs). An immense reflection from the BGs on the tip of an SMF and a high-birefringent PMF was revealed by a record value of reflection of over −22 dB with nearly no degradation of its polarization properties. Furthermore, a negligible amount in polarization sensitivity was observed when the BGs were deposited on the tip of PMFs.

2. Results and Discussion

2.1. Fabrication of Silicon Oxynitride-Doped Silicon Thin Films

Figure 1a,b shows the schematic of the fabrication of SiON-doped Si thin films and the polariscope images of two different samples fabricated at 80 and 200 °C. The polariscope images show qualitatively that the thin films grown at low and relatively high temperatures are generally strain-free. The respective FTIR spectra are shown in Figure 1c, which reveals the vibrational frequencies of the deposited structures of both thin films. At the fingerprint region at ≈760 and 902 cm^{-1}, Si–O–Si and Si–N–Si bonds were respectively observed. Since only the temperature in the growth recipe was changed, the FTIR results suggest qualitatively that the oxygen and the hydroxyl (the inset in Figure 1c) contents could be modified upon the fast cooling. The structures of the samples were also investigated using the Raman study demonstrated in Figure 1d. The broad peaks located at ≈475 and 477 cm^{-1} are the typical characteristics of the transverse optical (TO) phonon mode of a-Si, respectively, for S1 and S2. The shoulders at ≈340 and 405 cm^{-1} were assigned to the longitudinal acoustic (LA) and optic (LO) modes, respectively. **Figure 2**a,b show the scanning electron microscopy (SEM) micrographs that present the size and morphology of the thin films coated on the glass slides. The coating size increased slightly when the growth temperature decreased from 200 to 80 °C. The final morphological and elemental analyses on the thin film samples were performed using the high-resolution transmission electron microscopy (HR-TEM) technique. The sizes of S1 and S2 found by the HR-TEM studies shown in Figure 2c,d respectively confirm those found in the SEM micrographs. Furthermore, the structure of both samples presents an amorphous nature as no crystallinity was observed in the insets of Figure 2b. **Table 1** gives the elemental distributions of S1 and S2 recorded ≈20 nm below the surface. Decreasing the growth temperature was observed to yield an increase in the deposition of relatively more SiON in a-Si. This gives us control over the change of optical properties, such as altering the refractive index. Thus, the reflection properties of the samples of almost the same size could be modified. The findings shown till now suggest that the formation of silicon oxynitride homogeneously mixed inside an a-Si matrix at relatively low temperatures is possible and can be utilized in the manufacturing of optical components consisting of the novel structures such as Bragg gratings on rigid and optical fibers.

2.2. Design and Fabrication of Silicon Oxynitride-Doped Silicon Containing Bragg Gratings on Bulk Substrates

A typical Bragg grating consists of alternating layers of two materials with different refractive indices (**Figure 3**a). It is well known that the interference between the reflections of each layer occurs as the light propagates through these layers. When the parameters such as thickness and refractive index of each layer can be modified, customized reflections at various wavelengths and bandwidths are obtained. The thickness of the alternating layers can be calculated for the central wavelength λ_c using the following equation:[20]

$$\mathbf{n}_{S2}\mathbf{d}_{S2} = \mathbf{n}_{SiO_2}\mathbf{d}_{SiO_2} = \lambda_c/4 \quad (1)$$

Where n_{S2} and n_{SiO_2} are refractive indices of S2 and SiO_2 layers, whereas d_{S2} and d_{SiO_2} are the thickness of S2 and SiO_2 layers, respectively. Therefore, the central wavelength of the BGs was modified via increasing the thickness of the alternating layers since the effective refractive index of the layers was considered to be constant as the temperature was not changed during the fabrication of the BGs.

Table 2 shows the Si-based materials usually grown in a deposition chamber, such as those in plasma-enhanced chemical vapor deposition (PE-CVD), and their respective refractive indices at the C band of telecom wavelength. The refractive indices of S1 and S2 formed in the previous subsection are included for comparison. Figure 3b shows the SEM images of a BG formed by 11 alternating layers of SiON-doped Si based on the recipe for the sample S2 and SiO_2 that is designed and fabricated for the reflection centered at the telecom wavelengths. Figure 3c gives the total reflection of the BG on a glass slide ≈99% reflection at 1550 nm with a 3 dB bandwidth of ≈280 nm.

The FTIR and the XPS studies were further conducted to study the structure of the BG separately. **Figure 4**a shows the FTIR spectrum of the BG presenting the vibrational frequencies at ≈760 and 902 cm^{-1} assigned to Si–O–Si and Si–N–Si bonds[16] respectively. Since both S2 and SiO_2 consist of Si–O–Si bonds, an increase in the respective band was observed in the FTIR of the BG compared to that of a single layer of silicon oxynitride-doped silicon (S2) demonstrated in Figure 1c. The elemental analyses through the depth of the BG were conducted using the XPS studies. The XPS study shown in Figure 4b confirms the layer-by-layer deposition of S2 and SiO_2. The elemental distribution of S2 found by the XPS study is comparable to the size locally determined from the HR-TEM studies (Table 1).

To demonstrate the flexibility of the technique yielding the low-temperature formation of the SiON-doped Si layers for altering the central reflection wavelength of BGs, five newly designed BGs were fabricated (**Figure 5**a). The BGs on glass slides are named BG@840, BG@915, BG@1200, BG@Telecom, and BG@1840 whose high reflection spectra are shown in Figure 5b. The reflection spectra presented therein for the samples deposited on

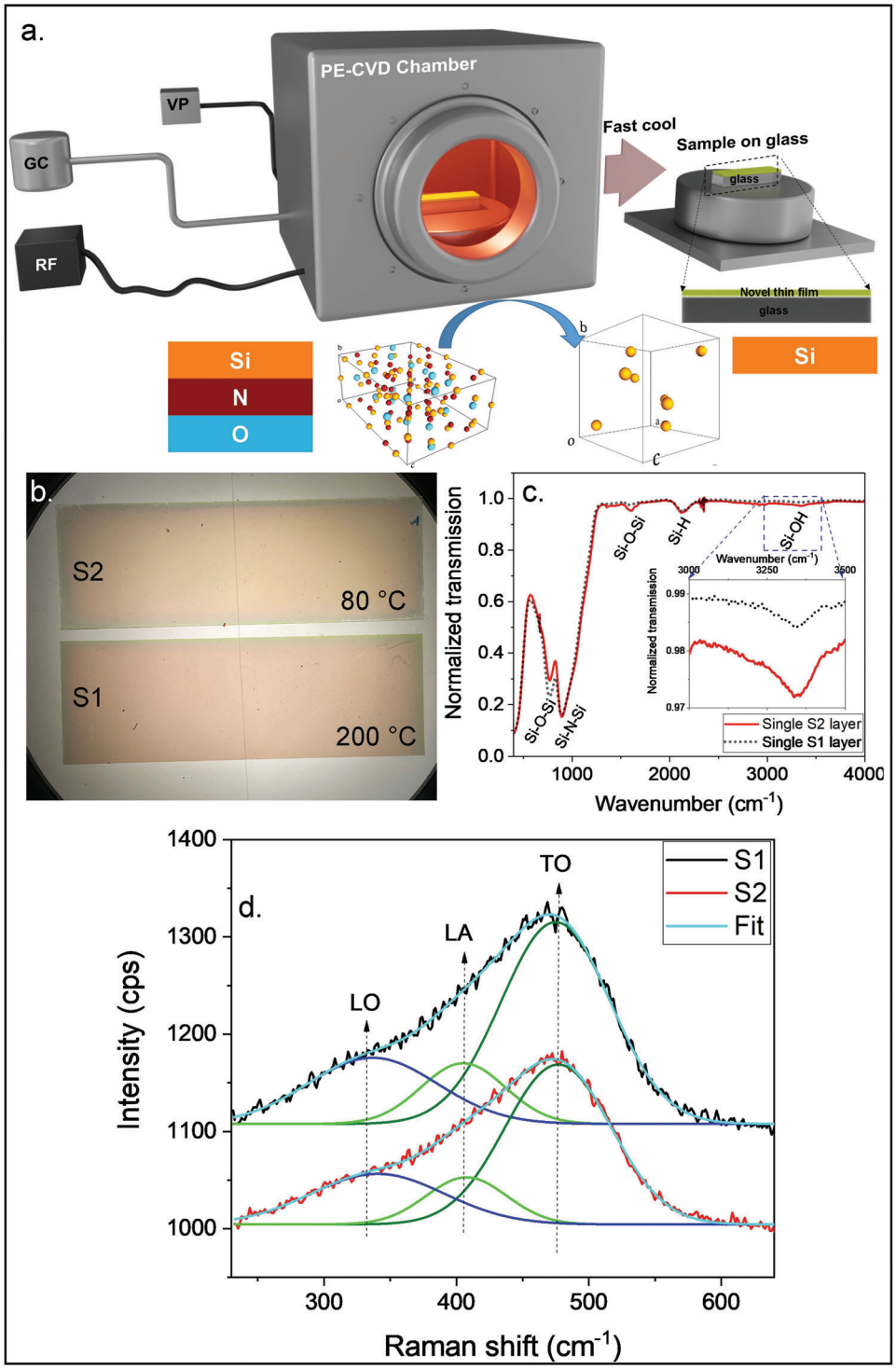

Figure 1. a) Schematic of synthesis of SiON-doped a-Si thin film on a rigid substrate and VP, GC, and RF stand for vacuum pump, gas cabinet, and radio-frequency generation unit. b) The polariscope images of the samples S1 and S2 on the glass slides c) the FTIR measurements of S1 and S2. d) The Raman spectra of S1 and S2. The deconvolutions of the Raman spectra are shown for the LO, LA, and TO modes using three Gaussian peaks at ≈340, 405, and 475 cm^{-1}.

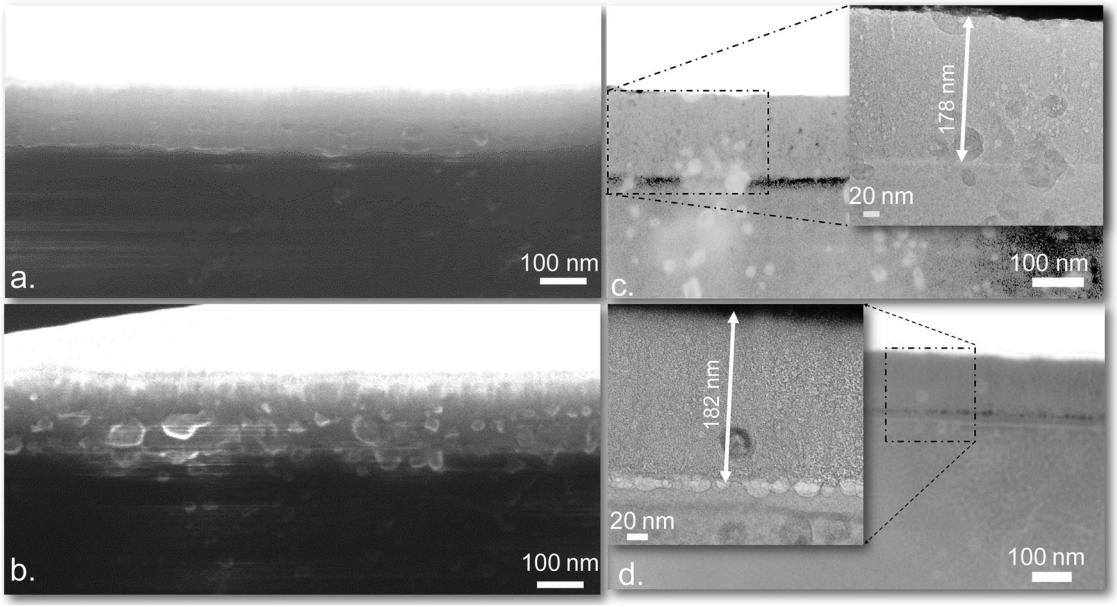

Figure 2. The SEM micrographs of a) S1 and b) S2. The HR-TEM micrographs of S1 and S2 are demonstrated in c,d) respectively for the precise size and amorphous nature (insets) of the thin films. The circular spots were formed due to e-beam sensitivity of the thin films.

Table 1. The elemental analyses of S1 and S2 were determined using the EDX in the HR-TEM in terms of the atomic percentage.

	%O	%N	%Si	Total
S1	11.5	8.6	79.9	100
S2	16.7	27.7	55.6	100

the borosilicate glasses were centered at the wavelengths from 800 to 1840 nm covering the NIR region over 2 μm due to the large bandwidth of BG@1840 nm being 660 nm. The respective 3 dB bandwidths were 272, 284, 433, 558, and 660 nm for BG@840, BG@915, BG@1200, BG@Telecom, and BG@1840. Furthermore, one of the fabricated BGs called BG@915 has a central reflection wavelength at 915 nm and was also grown on a SiO_2 substrate that has particular importance in combining diode lasers, high-power lasers, and multispectral lasers operated for 1-micron applications.[21–23] Both the application wavelengths such as pump wavelengths of 915 and 976 nm utilized in the generation of 1-micron lasers and the substrates that must be durable at high-power applications are critical for long-term and safe operation of the BGs. Watt-level reflection of laser light from BG@915 was tested at the wavelength of 976 nm acquired from a Yb-doped fiber laser. When the incident angle was $\leq 8°$, over 99% reflection was recorded. Figure 5c shows that the percentage of the reflected light is gradually filtered out at larger angles of the incident light till the level of ≈11% at the incident angle of 60°. The numerical simulations (Figure S1, Supporting Information) of the reflection from the BG suggest that the decrease in the reflection of the incident light occurs due to the shift of the reflection peak to the lower wavelength windows and causes the reflection at the wavelength of 976 nm. Therefore, the incident angle dependence provides tunability in the reflection properties of the BGs as well in addition to tunability of the reflection peak in the fabrication process. The BGs reported in this work are compatible with SOI technology and were also deposited on a Si wafer as shown in the inset of Figure 5d. The corresponding reflection spectrum centered at 915 nm demonstrates that the reflection data from BG@915onSi is quite similar can be designed and fabricated for different substrates widely utilized in the field. Nevertheless, the 3 dB bandwidth of from BG@915onSi was found to be 347 nm which is slightly larger than that of BG@915 fabricated on a borosilicate glass. Another important property of the fabricated BGs is the homogeneity when depositing the thin films. In order to determine the homogeneity, three different reflection measurements were conducted on the same sample (BG@Telecom). These measurements are presented in Figure 5e which demonstrates that Point 2 and Point 3 have an exact match in the reflection spectra, both of which have an insignificant deviation with respect to the reflection from Point 1. This small deviation is due to the presence of strains at the edge of BG@Telecom deposited on a borosilicate glass slide observed in the polariscope images in Figure 5a that almost disappeared when using thinner and larger substrates such as BG@915 on a 2-inch SiO_2 substrate.

2.3. Demonstration of Silicon Oxynitride-Doped Silicon Containing Bragg Gratings on the Tip of the Optical Fibers

Fabrication of the BGs on optical fibers is relatively challenging in a way that the BG is to be grown homogeneously on respectively smaller sizes compared to bulk substrates such as 125 μm cladding diameter. Therefore, the successful development of the designed BG depends not only on the growth parameters, including the plasma power and deposition temperature but also on the case of whether the fiber is bare or within the connector. **Figure 6**a,b reveal before and after the deposition of the BG on

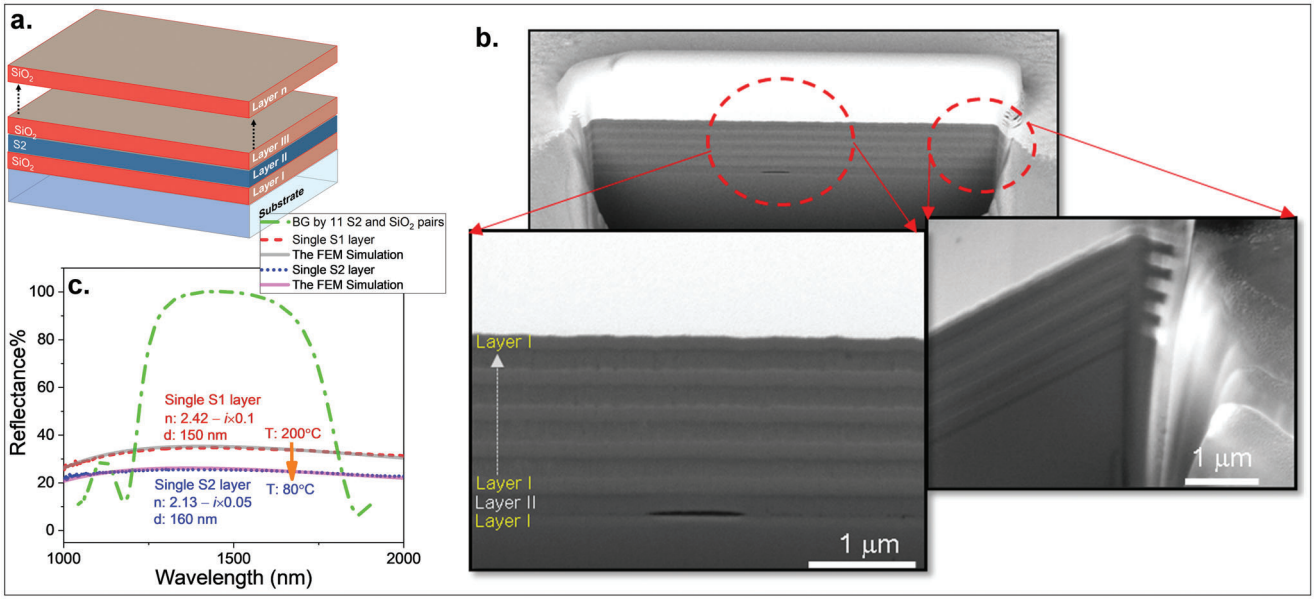

Figure 3. a) Schematic of fabrication of the BG using alternating layers of SiON-doped Si and SiO_2 on a substrate at low temperatures, b) The SEM images of the BG formed with the deposition of 11 subsequent layers of SiON-doped Si (S2) and SiO_2 on a glass slide is demonstrated. c) The reflection data of S1 and S2 on glass are compared with the numerical simulations using the finite element methods.

Table 2. The real component of the refractive indices of S1 and S2 compared with the other Si-based materials at 293 K.

	n@1550nm
SiO_2	1.4431 [30]
Si_3N_4	1.9827 [31]
SiO_xN_y	1.840–1.940 [32]
a-SiN_x	3.81-4.01[a] [26]
a-Si	3.480 [33]
c-Si	3.4757 [34]
S1	2.2690 (This work)
S2	2.0961 (This work)

[a] The measurement was conducted at 633 nm.

the SMF within the connector. The homogenous deposition was achieved on this occasion since the BG on the SMF within the connector gives a surface roughness (R_a) of ≈6 nm. In contrast, the vertical position of the bare fiber in the chamber becomes more critical when the fiber is bare. Figure 6c,d demonstrates the BG grown on the PM fiber for which a circular deposition of the BG was achieved with a surface roughness of ≈220 nm. Higher roughness suggests that the relaxation or the diffusion of the radicals from the plasma sheath (vapor) might not occur sufficiently[24] and the BG film on a bare PM fiber has more tendency to have a defect on its surface. Similarly, the BG on the SMF within the connector possesses more surface; thus, more time for the molecular groups for the relaxation and diffusion was provided and yielded a smooth film and a roughness of nearly two orders of magnitude smaller. The BGs were also deposited onto the ceramic connector surface that can be stripped via small physical forces such as peeling the BGs by sticky tapes.

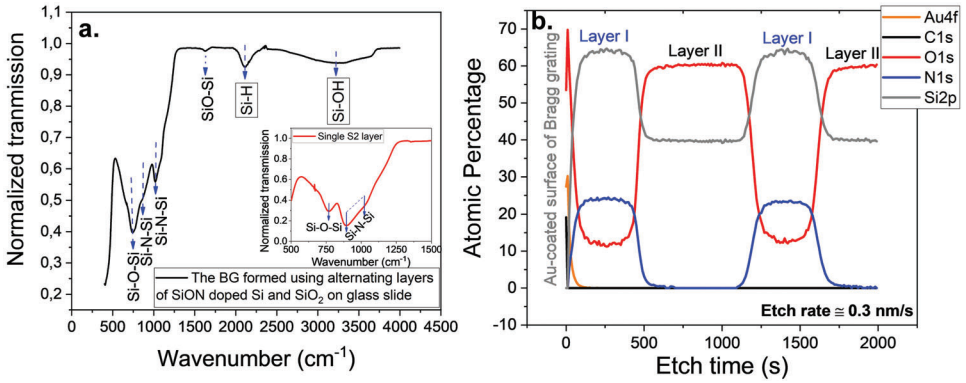

Figure 4. a) FTIR and b) XPS measurements of the BG formed by 11 subsequent layers of SiON-doped Si (S2 as layer 1) and SiO_2 (layer 2) on a glass slide. The inset in (a) shows the FTIR of S2 for the comparison with that of the BG.

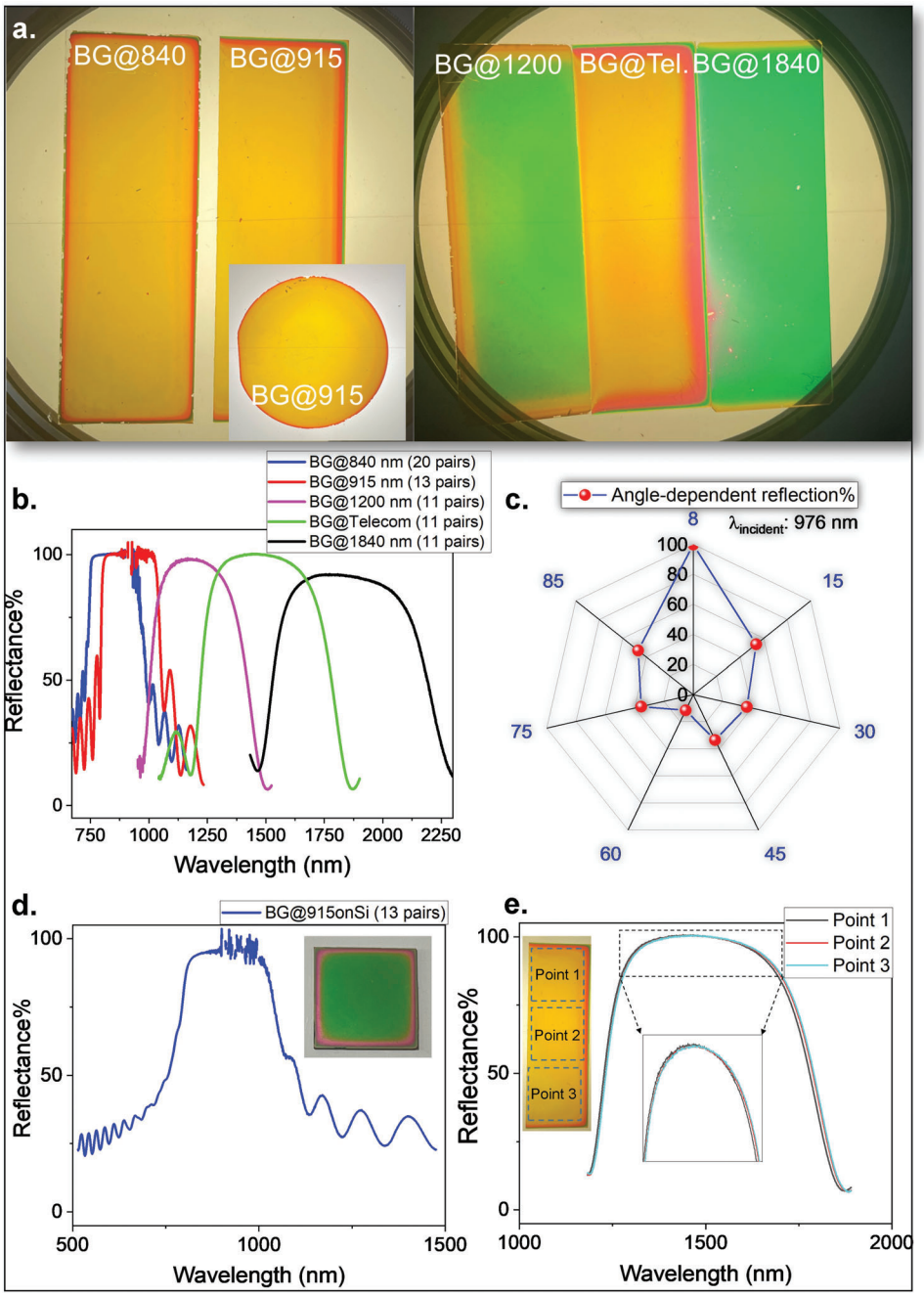

Figure 5. a) The optical images under the polariscope demonstrate the film homogeneity of five different BGs along the general-purpose borosilicate glass slides having a dimension of 25 × 75 mm. BG@915 is also shown on 2 inch SiO_2 glass with the optical image of ≈1 W reflected light. b) The experimental reflection data of the BGs from BG840 to BG1840 cover the reflection wavelength window from 750 to 2000 nm. c) The incident angle-dependent experimental reflection data of BG@915 on the silica glass shows the intensity dependence of the reflection on the incident angle of a continuous laser at the wavelength of 976 nm. d) The experimental reflection data of BG@915onSi and e) the reflection of BG@Tel. at three different points on the sample are demonstrated. The noise ≈1000 nm is due to the detector change in the UV–vis–NIR reflection measurements.

The performance of the BG deposition on the optical fibers was tested using the reflection and transmission configurations (**Scheme 1**a,b respectively). Figure 6e shows the reflection of the ASE light coupled to the SMF and the PMF that have ≈30 dB reflection with over a 24 dB difference in the reflection of the fiber without BGs. Total reflection of a BG structure is divided into two components including specular and diffuse reflection (Figure S2a, Supporting Information) in which the former refers to the mirror-like reflection having the reflection angle occurring at incident angle of the light. However, diffuse reflection can take place on the surfaces where inhomogeneities in the coating cause the reflection in many directions. The diffuse reflection

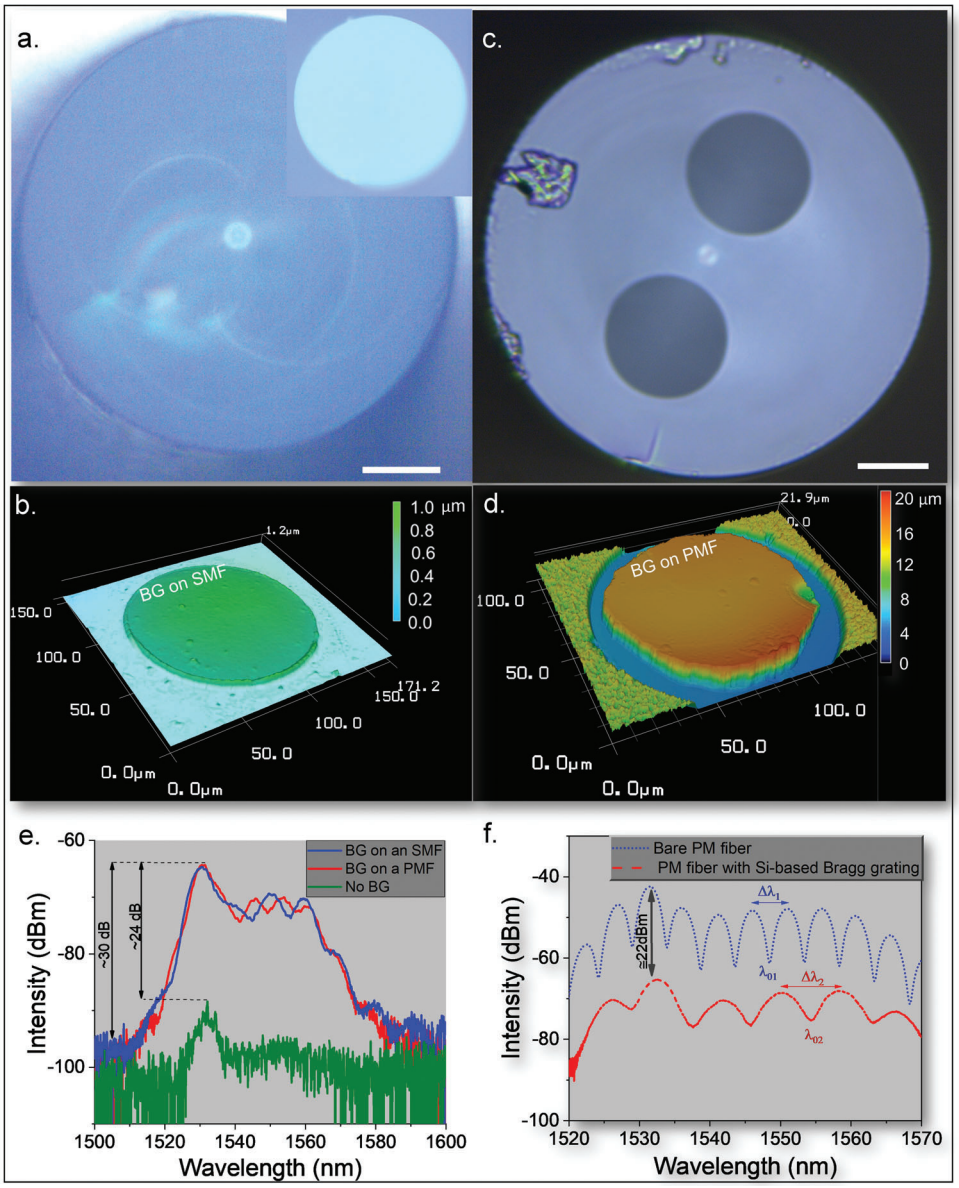

Figure 6. The cross sectional optical images of a) the bare SMF and b) the bare PMF in transmission mode. BG4 consisting of alternating layers of the SiON-doped Si and SiO_2 deposited on the tip of c) an SMF within a fiber connector and d) a PMF without connector. e) The respective reflectivity measurements of the amplified spontaneous emission from the BGs on the fibers compared to that without BGs. f) The transmission measurements with (dashes) and without (dots) BG4 on the tip of the PMF. The inset image in (a) shows the optical image of the SMF in reflection mode. The scale bars are 20 μm.

measurement was conducted for S2 to estimate the portion of the reflection that could occur due to other effects such as scattering. In Figure S2b (Supporting Information), the diffuse reflection from a single SiON-doped Si film was shown to be ≈0.5% (≈−0.02 dB) that confirms most of the reflection (at least ≈−22 dB) in the optical fibers is due to specular component and Bragg-mirror property of the fabricated BGs on optical fibers.

To test the BG on the PM fiber, a polarized incident light was first launched at 45° angles with respect to the major axis of a PM fiber (slow axis) without the BG as reported in detail in our previous study.[25] Briefly, polarization properties of a PM fiber, including the beat length and/or birefringence, are reported in general to demonstrate its high birefringence. Figure 6f shows the $\Delta\lambda$ values corresponding to the separation between the two adjacent maxima at the wavelengths from 1520 to 1580 nm, comprising the telecom S-C-L bands. Considering the length, L of two PM fibers (the pristine and the BG deposited) are the same ($L = 1m$), observing the separation between two adjacent peaks would directly reveal how the polarization properties altered when the BG deposited on the PM fiber. The pristine PM fiber was determined to have a beat length of 0.95 mm and birefringence of 1.63×10^{-3} at the central wavelength of 1551.0 nm. Depositing the BG on the PM fiber yields that the PM fiber still retains its high-birefringent property that gives a beat length of 1.68 mm and birefringence of

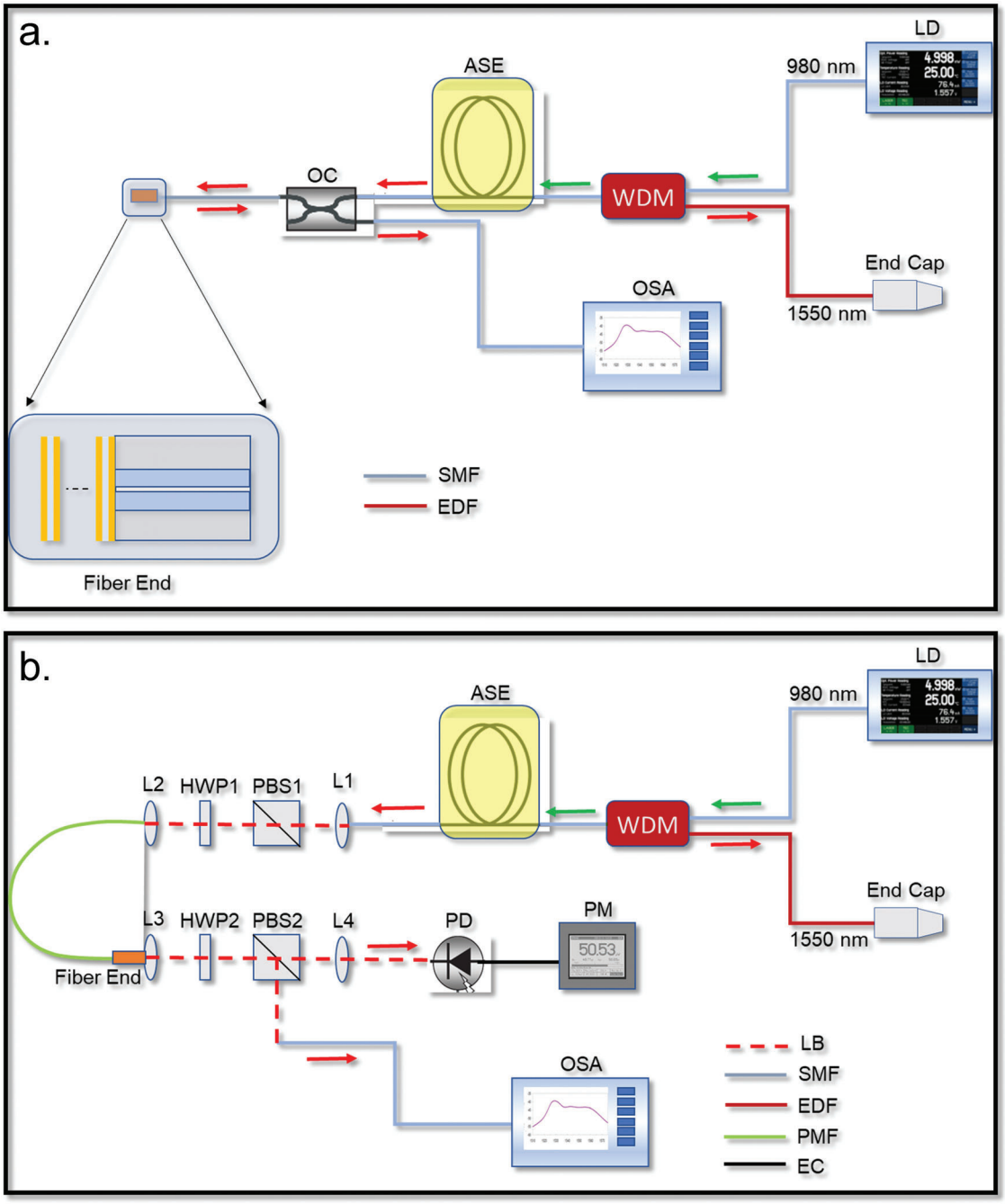

Scheme 1. The optical set-ups for determination of the performance of the BGs on the tip of a) an SMF and b) a PMF. LD is a laser diode that operates at 980 nm; WDM is a 1550/980 nm wavelength division multiplexer; EDF is erbium-doped fiber; SMF is a single-mode optical fiber; ASE is an amplified spontaneous emission; OC is an optical coupler; L1, L2, L3, and L4 are lenses used for focussing and collimating the light; PBS1 and PBS2 are polarization beam splitters; HWP1 and HWP2 are half-wave plates; PD is a photodiode; PM is a power meter; OSA is an optical spectrum analyzer. LB is laser beam, SMF is single-mode optical fiber, EDF is Er-doped optical fiber, PMF is polarization-maintaining fiber, and EC is electrical cable.

0.92×10^{-3} at the central wavelength of 1550.4 nm. Despite the fact that the amorphous nature of the structure of the BGs determined from Raman and HR-TEM studies, such small change in the PM properties could be a sign for the presence of minute crystallites that could be detected via further advanced characterization techniques such as synchrotron radiation probes.

3. Conclusion

The syntheses of SiON-doped a-Si were shown on bulk substrates via the low-temperature PE-CVD technique. It gives control in the refractive index of the deposited structure that was further utilized in the creation of BGs for the high-reflection of light at

different wavelengths not only on bulk substrates but also on different fiber facets such as SMFs and PMFs. The fabrication technique reported here shows the BGs at different substrates can be fabricated homogeneously on different substrates and μ-scale optical fibers. The direct deposition of BGs on the fiber tips provided over −22 dB reflection with these fibers and yielded to preserve its high birefringent property when coated on the PM fiber tip. This novel technique is promising for the preparation of bulk samples and fiber tips equipped with the novel BGs that are utilized for different Si-based waveguides and photonics applications, including optoacoustic, mode-locking, and spectral sensing.

4. Experimental Section

Fabrication—Fabrication of Silicon-Oxynitride Doped Silicon Thin Films: The bulk substrates were cleaned with a sequence of acetone, ethanol, and isopropyl alcohol, and dried by blowing N_2 Similarly, the tips of optical fibers were cleaned only by isopropyl alcohol, and dried by blowing N_2 due to the prevention of the possible damage to the polymer coatings of the optical fibers. Silicon-oxynitride doped silicon thin film was synthesized using a new method developed within PE-CVD method (Model: Advanced Vacuum Vision 310) using precursors SiH_4/N_2 (2%/98%) under a relatively low plasma power of 100 W with a radio frequency (RF) of 13.56 MHz under a vacuum $\approx 10^{-5}$ mBar and fast cooled under the ambient atmosphere as schematically demonstrated in Figure 1a. After the synthesis, the fast-cooling process was initiated that involves quickly releasing the PE-CVD chamber cover to the ambient temperature of 18 °C in the clean room and the substrates and optical fibers were collected from the heating stage instantly. The cooling rate was determined to be ≈ 5 °C s^{-1} which was found by measuring the temperature change using a thermal camera (Model: FLIR System A40). The fast-cooling process provided quick access to the fabricated thin films without degradation to the film quality with small Ra values that gives an opportunity for the mass-scale fabrication of the thin films and the optical devices.

Fabrication—Fabrication of Silicon-Oxynitride Doped Silicon-Containing Bragg Gratings: Bragg gratings on different substrates, including borosilicate and silica glasses, were formed using alternating layers of silicon-oxynitride doped silicon and silica deposited at relatively low temperatures, ≈80 °C and a plasma power of 100 W. The SMFs were in general coated with the UV-curable acrylic polymers that can withstand the ambient temperatures until 85 °C, therefore, the low-temperature synthesis method reported in this study provides a cost-effective route for the preparation of the high-reflection BGs on fibers over −22 dB

Fabrication—Fabrication of Silicon Oxynitride-Doped Silicon Containing Bragg Gratings on Optical Fibers: The Bragg gratings developed in the previous step were also deposited on the tip of optical fibers, including an SMF and a PMF (Models: Fujikura G-652 D and Corning PM 980 respectively). An SMA 905 connector was utilized when the BGs were deposited on the SMF within the connector. The optical fibers were coated with and without connectors. The fibers without connectors were cleaned with isopropyl alcohol before cleaving and then cleaved with a cleaver (Model: Fujikura CT-32 for SMFs and Fujikura CT-105 for PMFs). After each cleaving process, the cleaving quality was checked by an optical microscope (Model: Zeiss Axio) before inserting the optical fibers into the PE-CVD chamber.

Characterization—Optical, Morphological, and Structural Characterizations: A polariscope (Model: Optacore POL-02) was used to record the optical images of thin films and Bragg gratings on rigid substrates between two polarizer films under white light. The UV–vis–NIR reflection measurements were collected using a Carry 5000 UV–vis–NIR Spectrometer with a range between 200 to 2500 nm with a step of 1 nm and a one-beam configuration. For the baseline reflection, a PTFE reference provided with the instrument was used within the same measurement window. For the determination of the refractive index of the thin films S1 and S2, variable angle ellipsometry (Model: J.A. Woollam Co. Inc.) was utilized within a spectral range from 800 to 1700 nm. The measurements were collected at the angles of the incident light from 60° to 80° with 5° steps. The dispersion relations Psi ($\psi(\lambda)$) and Delta ($\Delta(\lambda)$) were measured and Kramers–Krönig model fitting[26] and Cauchy model fitting[27] were used to find the thickness and the optical indices of n and k, respectively for SiON-doped Si and SiO_2. A focused ion beam within HR-SEM (Model: FEI Nova NanoSEM 600i) was used to etch and then record the cross sectional SEM micrographs of Bragg gratings. The FTIR measurements were performed at ATR (4000–400 cm^{-1}) region using an FTIR ATR spectrometer (Thermo Fisher Scientific). A Raman spectroscopy (Model: Witec SNOM Raman 300 Alpha coupled with a diode laser at $\lambda = 532$ nm) technique was utilized for the further structural analysis of the thin films (S1 and S2) using a grating with the groove density of 600 g mm^{-1}. The phonon modes for the LO, LA, and TO modes were obtained from the least squares fit of Gaussian peaks located at ≈340, 405, and 475 cm^{-1} following the previous studies.[28,29] Thermo, USA (Kα-monochromated high performance) in an ultra-high vacuum (UHV) with a conventional X-ray source (Mg-Kα) was utilized for the X-ray photoelectron spectroscopy (XPS) technique. The charge-shift correction was conducted for the XPS measurements using C 1s (284.8 eV) level.

Characterization—Optical Characterizations of Bragg Gratings on Fibers: The set-ups in Scheme 1 were built and operated to determine the reflection of BGs on the optical fibers, including on the SMF (Scheme 1a.) and the PMF (Scheme 1a,b). For the BG on the PMF, the reflection was also determined from the transmission measurement. A backscattered amplified spontaneous emission (ASE) was formed by a 980/1550 nm wavelength division multiplexer (WDM) with HI1060 fiber connectors, and 1.5 m of an Er-doped fiber (Model: Liekki 20 Er80-8/125). The W-level setup consisted of a pumping diode (Model: Lumentum 10 W fiber-coupled diode laser at $\lambda = 976$ nm, $NA = 0.22$, operated power = 1.0 W) integrated by a pump combiner, a DC power supply, a power meter (Model: Thorlabs PM200) all located on an optical table. In the reflection measurement scheme, light was coupled to the BG on fiber using a 2×1 coupler and collected from the other arm of the coupler, and recorded with a power meter (Model: FieldMaxII) and optical spectrum analyzer (OSA, Model: Yokogawa AQ6370C).

Numerical Analysis: A finite element method using COMSOL Multiphysics 5.0 was used for numerical analyses of the reflection measurements of Bragg gratings. The parameters utilized in the simulations are provided in Table S1 (Supporting Information). The refractive indices of each layer including silicon oxynitride-doped silicon and silicon dioxide were obtained from the experimental ellipsometry measurements.

Supporting Information

Supporting Information is available from the Wiley Online Library or from the author.

Acknowledgements

This work was supported by the Scientific and Technological Research Council of Turkey (TÜBİTAK) ARDEB 3501 Career Development Program under the Project No. 121F255 and BİDEB-National Postdoctoral Research Program under the Project No. 118C541. The authors also acknowledge infrastructural support provided by National Nanotechnology Research Center (UNAM) at Bilkent University and TENMAK BOREN.

Conflict of Interest

The authors declare no conflict of interest.

Data Availability Statement

The data that support the findings of this study are available from the corresponding author upon reasonable request.

Keywords

Bragg gratings, high birefringence, low-temperature synthesis, optical fibers, silicon oxynitride, waveguides

Received: January 13, 2023
Revised: February 26, 2023
Published online: April 4, 2023

[1] A. G. Cullis, L. T. Canham, *Nature* **1991**, *353*, 335.
[2] J. C. Philips, J. C. Bean, B. A. Wilson, A. Ourmazd, *Nature* **1987**, *325*, 121.
[3] R. Adar, C. H. Henry, R. C. Kistler, R. F. Kazarinov, *Appl. Phys. Lett.* **1992**, *60*, 1779.
[4] E. Chomski, G. A. Ozin, *Adv. Mater.* **2000**, *12*, 1071.
[5] A. Birner, R. B. Wehrspohn, U. M. Gösele, K. Busch, *Adv. Mater.* **2001**, *13*, 377.
[6] R. Soref, *IEEE J. Sel. Top. Quantum Electron.* **2006**, *12*, 1678.
[7] J. Ferrara, W. Yang, L. Zhu, P. Qiao, C. J. Chang-Hasnain, *Opt. Express* **2015**, *23*, 2512.
[8] B. Tian, Z. Wang, M. Pantouvaki, P. Absil, J. Van Campenhout, C. Merckling, D. Van Thourhout, *Nano Lett.* **2017**, *17*, 559.
[9] S. Khajavi, D. Melati, P. Cheben, J. H. Schmid, C. A. A. Ramos, W. N. Ye, *Sci. Rep.* **2022**, *12*, 18808.
[10] N. Singh, M. Raval, E. Ippen, M. R. Watts, F. X. Kärtner, *Appl. Phys. Lett.* **2021**, *118*, 071106.
[11] Y. Hazan, A. Levi, M. Nagli, A. Rosenthal, *Nat. Commun.* **2022**, *13*, 1488.
[12] A. Boes, B. Corcoran, L. Chang, J. Bowers, A. Mitchell, *Laser Photonics Rev.* **2018**, *12*, 1700256.
[13] Q. Li, M. Davanço, K. Srinivasan, *Nat. Photonics* **2016**, *10*, 406.
[14] E. Ryckeboer, X. Nie, A. Dhakal, D. Martens, P. Bienstman, G. Roelkens, R. Baets, in *2017 IEEE 14th Int. Conf. Gr. IV Photonics*, IEEE, Piscataway, NJ **2017**.
[15] P. Temple-Boyer, B. Hajji, J. L. Alay, J. R. Morante, A. Martinez, *Sensors Actuators, A Phys.* **1999**, *74*, 52.
[16] M. I. Alayo, I. Pereyra, W. L. Scopel, M. C. A. Fantini, *Thin Solid Films* **2002**, *402*, 154.
[17] L. Picelli, A. Van Klinken, G. Lindgren, K. D. Hakkel, F. Pagliano, N. Fiaschi, I. Sersic-Vollenbroek, P. J. Van Veldhoven, R. W. Van Der Heijden, A. Fiore, *Appl. Phys. Lett.* **2020**, *117*, 151101.
[18] K. D. Hakkel, M. Petruzzella, F. Ou, A. van Klinken, F. Pagliano, T. Liu, R. P. J. van Veldhoven, A. Fiore, *Nat. Commun.* **2022**, *13*, 103.
[19] L. Orsila, R. Herda, O. G. Okhotnikov, *IEEE Photonics Technol. Lett.* **2007**, *19*, 2009.
[20] X. Ding, C. Gui, H. Hu, M. Liu, X. Liu, J. Lv, S. Zhou, *Appl. Opt.* **2017**, *56*, 4375.
[21] I. V. Ciapurin, L. B. Glebov, V. I. Smirnov, *Fiber Lasers Technol. Syst. Appl.* **2004**, *5335*, 116.
[22] A. Mirigaldi, V. Serafini, P. Gotta, G. Pippione, C. Coriasso, R. Paoletti, G. Perrone, in *High-Power Diode Laser Technol. XVIII*, (Ed.: M. S. Zediker), SPIE, Bellingham, WA **2020**.
[23] R. Paschotta, J. Nilsson, A. C. Tropper, D. C. Hanna, *IEEE J. Quantum Electron.* **1997**, *33*, 1049.
[24] G. R. Yang, Y. P. Zhao, Y. Z. Hu, T. P. Chow, R. J. Gutmann, *Thin Solid Films* **1998**, *333*, 219.
[25] A. Karatutlu, E. Y. Yıldırım, E. Kendir, Y. Midilli, S. Akçimen, B. Ortaç, *Opt. Fiber Technol.* **2022**, *69*, 102836.
[26] J. Jaglarz, M. Jurzecka-Szymacha, S. Kluska, *Thin Solid Films* **2019**, *669*, 564.
[27] D. Hohlfeld, H. Zappe, *J. Opt. A: Pure Appl. Opt.* **2004**, *6*, 504.
[28] F. Kohler, T. Zimmermann, S. Muthmann, A. Gordijn, R. Carius, *IEEE J. Photovoltaics* **2014**, *4*, 4.
[29] M. H. Brodsky, M. Cardona, J. J. Cuomo, *Phys. Rev. B* **1977**, *16*, 3556.
[30] J. Kischkat, S. Peters, B. Gruska, M. Semtsiv, M. Chashnikova, M. Klinkmüller, O. Fedosenko, S. Machulik, A. Aleksandrova, G. Monastyrskyi, Y. Flores, W. T. Masselink, *Appl. Opt.* **2012**, *51*, 6789.
[31] L. Y. Beliaev, E. Shkondin, A. V. Lavrinenko, O. Takayama, *Thin Solid Films* **2022**, *763*, 139568.
[32] Y. Wang, X. Cheng, Z. Lin, C. Zhang, F. Zhang, *Vacuum* **2003**, *72*, 345.
[33] D. T. Pierce, W. E. Spicer, *Phys. Rev. B* **1972**, *5*, 3017.
[34] H. H. Li, *J. Phys. Chem. Ref. Data* **1980**, *9*, 561.